Nuclear Science and Techniques (2025) 36:134
https://doi.org/10.1007/s41365-025-01728-x

Exploring the multiplicity dependence of the flavor hierarchy for hadron production in high-energy pp collisions

Ao-Gui Zhang[1] · Xin-Ye Peng[1,2] · Liang Zheng[1,3]

Received: 25 October 2024 / Revised: 19 January 2025 / Accepted: 21 January 2025 / Published online: 2 June 2025

Abstract

In this study, we performed a systematic analysis of the multiplicity dependence of hadron production at mid-rapidity ($|y| < 0.5$), ranging from the light to the charm sector in proton–proton (pp) collisions at $\sqrt{s} = 13$ TeV. This study used a multi-phase transport (AMPT) model coupled with PYTHIA8 initial conditions. We investigated the baryon-to-meson and the strange-to-non-strange meson ratios varying with the charged particle density. By tuning the coalescence parameters, the AMPT model provides a reasonable description of the experimental data for the inclusive production of both light and charm hadrons, comparable to the string fragmentation model calculations with color reconnection effects. Additionally, we analyzed the relative production of hadrons by examining the self-normalized particle ratios as a function of the charged hadron density. Our findings suggest that parton evolution effects and the coalescence hadronization process in the AMPT model result in a strong flavor hierarchy in the multiplicity dependence of the baryon-to-meson ratio. Furthermore, our investigation of the p_{T} differential double ratio of the baryon-to-meson fraction between high- and low-multiplicity events revealed distinct modifications to the flavor associated baryon-to-meson ratio p_{T} shape in high-multiplicity events when comparing the coalescence hadronization model to the color reconnection model. These observations highlight the importance of understanding the hadronization process in high-energy pp collisions through comprehensive multiplicity-dependent multi-flavor analysis.

Keywords Heavy flavor · Multiplicity dependence · Small system · AMPT

1 Introduction

Collective phenomena have long been considered crucial signatures for the formation of a deconfined state of nuclear matter, quark–gluon plasma (QGP), in high-energy heavy-ion collisions [1–5]. However, in recent years, a flood of similar collectivity-like features has been observed in smaller systems, namely, high-multiplicity proton–proton (pp) and proton–nucleus (pA) interactions at the Relativistic Heavy-Ion Collider and Large Hadron Collider (LHC) [6–12]. These findings, which are largely unanticipated for such small systems, indicate potential similarities between the collective behaviors observed in small and large systems, demanding a paradigm shift in our understanding of QGP [13, 14]. Investigating the system size dependence of these collectivity phenomena is an important way to understand the properties of deconfined quark matter created during different collision processes.

The system sizes of different collisions can be effectively classified based on the event multiplicity, frequently represented by the final-state charged-particle pseudo-rapidity density measured at mid-rapidity $\mathrm{d}N/\mathrm{d}\eta$ [15–18]. Variations in hadron yields related to particle species [16, 19, 20] and characteristic shifts in p_{T}-dependent baryon-to-meson ratios

This work was supported by the National Natural Science Foundation of China (Nos. 12205259 and 12147101) and the Fundamental Research Funds for the Central Universities, China University of Geosciences (Wuhan) with No. G1323523064.

✉ Liang Zheng
zhengliang@cug.edu.cn

[1] School of Mathematics and Physics, China University of Geosciences (Wuhan), Wuhan 430074, China

[2] Key Laboratory of Quark and Lepton Physics (MOE) and Institute of Particle Physics, Central China Normal University, Wuhan 430079, China

[3] Shanghai Research Center for Theoretical Nuclear Physics, NSFC and Fudan University, Shanghai 200438, China

[11, 16, 19, 21] with different final-state multiplicities are remarkable initial sparks, indicating the existence of the collectivity effect identified in small systems. A continuous transition of hadron production as a function of $\mathrm{d}N/\mathrm{d}\eta$ has been observed from pp collisions to much heavier ion collisions [9, 11]. The smooth evolution of the yield and abundance of different hadron species suggests the existence of a common underlying mechanism that determines the chemical composition of the particles produced in these different collision systems.

Distinguishing modifications to the hadron production process, such as baryon-to-meson fraction changes, were initially investigated using hadrons consisting of light-flavor quarks. The resemblance of light-flavor hadron production between high-multiplicity pp and heavy-ion collisions in the soft regime stimulates the application of hydrodynamic and thermodynamic modeling to describe bulk particle yields in small systems [22–28]. The measured relative abundances of the created particles can be used as important experimental inputs to constrain the temperature, chemical potential, and volume of the matter produced in pp collisions [29–32]. Another phenomenological modeling approach often relies on a modified string fragmentation framework implemented based on the multi-parton interaction (MPI) assumption [33–38]. Researchers expect that inter-string effects can be sizable in a dense environment with multiple MPI string systems overlapping in the coordinate space. The color reconnection and rope hadronization effects implemented in the PYTHIA8 model successfully described the multiplicity dependence of the flow-like behavior of particle spectra in pp collisions [33, 39, 40].

Recently, similar multiplicity-dependent measurements have been extended to charm hadrons in high-energy pp collisions, and a sizable enhancement of the baryon-to-meson ratio Λ_c^+/D^0 at intermediate p_T has also been observed [41, 42]. Unlike light-flavor hadrons, charm hadrons are frequently produced through the hadronization of charm quarks originating from the initial hard-scattering process. The significant differences in the charm quark fragmentation fractions observed in LHC pp collisions compared with those in electron–positron and electron–proton collisions have been surprising. The origin of these discrepancies is currently being debated [41, 43, 44]. Calculations based on PYTHIA8 using fragmentation parameters tuned to electron–positron and electron–proton collisions cannot describe this charm hadron production characteristic in pp collisions. However, the PYTHIA8 results with the color reconnection effect were found to provide much better agreement with the experimental data [41, 42, 45]. Models that consider the coalescence mechanism for charm quark fragmentation can also satisfactorily reproduce the experimental data, assuming the creation of deconfined quark matter in a small system [46–50]. This array of hadron production measurements across the flavor spectrum indicates the necessity of modifying the fragmentation process in vacuum. A systematic study to understand the multiplicity dependence of the flavor hierarchy can be of significant benefit in differentiating the underlying explanations for the flow-like effects in pp collisions.

In this work, we employed the string-melting AMPT model built on PYTHIA8 initial conditions, including the final-state interactions and parton coalescence mechanism, to study the multiplicity-dependent hadron production of various flavors. The AMPT model with PYTHIA8 initial conditions was observed to describe the hadron yield in the soft regime and multiparticle correlations reasonably well [51, 52]. Being capable of delivering the final-state rescattering effects at both partonic and hadronic levels, the AMPT model provides an important method to test the final-state effects for hadron production from light to heavy flavors in the presence of deconfined parton matter. We compared the AMPT results to the string fragmentation model calculations in the multiplicity-dependent flavor hierarchy of hadron production to demonstrate the key features of these two widely used physics assumptions for small system collectivity studies.

The remainder of this paper is organized as follows: we explain the model setups for the AMPT model and the color reconnection included string fragmentation model in Sect. 2. The results of the model calculations are presented and compared with experimental data in Sect. 3. We summarize the major conclusions and discuss future applications in Sect. 4.

2 Method

In this study, we used the AMPT model based on the PYTHIA8 initial conditions to explore the final-state interaction effects on hadron production with different flavor components. The string-melting AMPT model consists of four major components: fluctuating initial conditions, final-state parton transport interactions, a coalescence hadronization model, and final-state hadronic cascade interactions. The event-by-event fluctuating initial conditions for the subsequent evolution stage were generated using PYTHIA8 [53] embedded with the spatial structure at the sub-nucleon level. After propagating the initial string system to their formation time and converting them to the constituent valence quark components, the resultant quark system may experience the parton evolution stage with the microscopic scattering process implemented by Zhang's parton cascade (ZPC) model [54], with a two-body scattering cross section σ frequently determined by comparison with anisotropic flow data. In this study, the value of the parton scattering cross section was set to $\sigma = 0.15$ mb which provides a satisfactory description of the elliptic flow measurements in pp collisions at $\sqrt{s} = 13$ TeV [55]. When partons cease their interactions

during the evolution stage, they combine with their nearby quarks using an improved spatial coalescence model [56]. An overall coalescence parameter r_{BM} has been introduced to determine the relative probability of a quark becoming a meson or baryon in this model. To describe the hadron yield for particles with different quark flavors, we followed the prescriptions in Refs. [51, 57, 58] and adjusted the coalescence parameters for each flavor sector. For non-strange light-flavor quark clusters, we set the coalescence parameter $r_{\mathrm{BM}} = 0.53$. If a strange or charm quark is involved in the coalescence process, the value of this parameter changes to $r^{\mathrm{s}}_{\mathrm{BM}} = 0.9$ and $r^{\mathrm{c}}_{\mathrm{BM}} = 1.4$, respectively. As discussed in Sect. 3, these choices can result in a reasonable description of the inclusive production for all investigated hadron species. After coalescence, the hadrons may undergo further hadronic rescattering, as described by the extended relativistic transport (ART) model [59, 60]. Note that the coalescence parameters may significantly influence the magnitude of the baryon-to-meson ratio globally; however, they do not introduce strong multiplicity dependence. In contrast, the fraction of the initial strings surviving the parton evolution stage also impacts the final hadron production ratios. The hadron ratios produced from the initial strings without participating in the evolution of the ZPC stage reflect the characteristics of the string fragmentation feature. In low-multiplicity events, hadronization from these non-interacting initial strings plays a significant role in hadron production. Conversely, in high-multiplicity events, coalescence is the dominant factor in determining the particle ratio. This interesting feature provides valuable insights into the collision system and its hadronization mechanism.

In this study, we turned on the parton and hadron final-state transport mechanisms in a step-by-step manner to explore the effects developed in different evolution stages. When both parton and hadron rescattering were disabled, the results were labeled as “noFSI" (no final-state interaction), whose behavior should be similar to the pure PYTHIA string fragmentation predictions without any collective effect. If the parton rescattering stage was enabled while hadron rescatterings are excluded, it was denoted as the “pFSI" case (partonic final-state interaction). When both final-state parton and hadron rescattering effects were included, the results were indicated as “allFSI" (all final-state interaction), in which the evolving system experienced the entire partonic and hadronic evolutions.

Collectivity-like behavior in small systems can also be induced by modified string fragmentation models that consider inter-string effects when a significant number of string pieces overlap in the limited transverse space [39]. The color reconnection (CR) model has been found to reasonably reproduce inclusive baryon-to-meson ratios with different flavors [37, 40, 42, 45]. In this study, we employed the beyond leading color (BLC) CR model built in the PYTHIA8.309 package [53], in which strings are allowed to form between both leading and non-leading connected partons [61]. With the possibility of forming junctions in BLC CR as an additional source for baryon production, multiplicity-dependent baryon enhancement is observed in this model [33]. We compared the AMPT calculations with the results from the CR model to explore the difference between these two underlying physical mechanisms. The parameters of the CR model used in this study were set by following the procedure described in Ref. [40, 62].

3 Results

This work focused on the hadron productions in pp collisions with $\sqrt{s} = 13$ TeV at mid-rapidity ($|y| < 0.5$) for eight different particle species: $\pi^{\pm}$, $K^{\pm}$, p($\bar{p}$), $\Lambda(\bar{\Lambda})$, K^0_{S}, D^0, $D^{\pm}_{\mathrm{s}}$, and $\Lambda^{\pm}_{\mathrm{c}}$. In Sect. 3.1, we present the inclusive productions and their ratios for these particle species in minbias events from the AMPT and PYTHIA color reconnection models, with comparisons to the ALICE experimental data [41, 63]. The multiplicity-dependent structures of these particle species ratios are further examined in Sect. 3.2 and Sect. 3.3. The events are classified based on the number of particles accepted by the ALICE V0 detector within the pseudo-rapidity regions $-3.7 < \eta < -1.7$ and $2.8 < \eta < 5.1$ following the prescription in Refs. [16, 19]. The production of these identified particles was studied with respect to the variation in charged particle density in each event class using the same percentile definition. To illustrate the final-state interaction effects embedded in the AMPT model, we present a comparison of the AMPT results with parton and hadron transport stages switched on, sequentially labeled noFSI, pFSI, and allFSI.

3.1 Inclusive particle production

The data for all light-flavor particles in this paper represent the sum of particles and anti-particles, whereas the data for heavy-flavor particles are the sum of particles and anti-particles divided by 2, following experimental analysis conventions. For inclusive hadron production, events were selected according to the minbias trigger used in the ALICE experiment, which requires signals accepted by either side of the V0 detector. The transverse momentum spectra for charged pions, kaons, and protons with $|y| < 0.5$ are shown in Fig. 1 produced in inelastic pp collisions at $\sqrt{s} = 13$ TeV. We observe that the ALICE data of the pion and kaon spectra can be roughly described by the allFSI model, with a slight overestimation of the pion production at p_{T} of approximately 1 GeV/c. In contrast, the proton spectra were overestimated by the allFSI model with p_{T} above 1.5 GeV/c. The overestimation of protons occurred because the current coalescence model in AMPT can

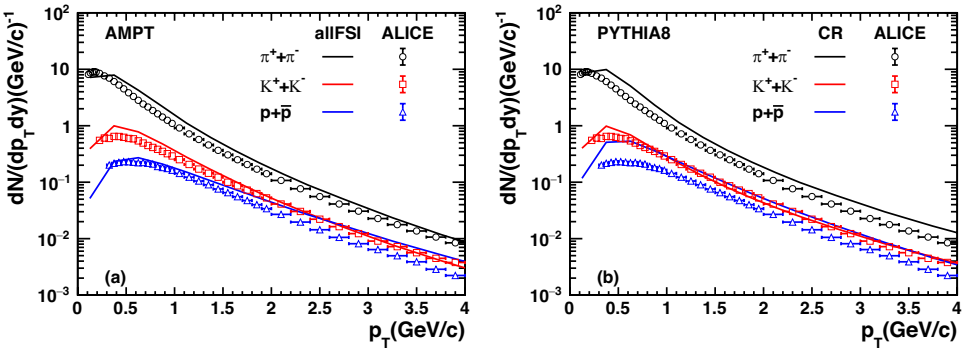

Fig. 1 (Color online) Transverse momentum spectra of charged $\pi^{\pm}$ (black), $K^{\pm}$ (red), and $p+\bar{p}$ (blue) in $\sqrt{s}=13$ TeV pp collisions at mid-rapidity $|y|<0.5$. The lines represent model calculations from AMPT with all final-state interactions (**a**) and PYTHIA8 model with color reconnection effects (**b**), whereas the open markers represent ALICE data [63]

affect hadrons even in the high-p_{T} region. Coalescence overpredicted the baryon spectra at high p_{T} because it assumed that quarks combined directly by adding their momenta, neglecting the dominance of fragmentation at high p_T, where baryon production became less efficient. In addition, hadronic rescattering, which induced radial flow-like effects to the proton spectra, enhanced proton production at higher p_{T}. Similar comparisons are presented in Sect. 3.3. The CR model results reasonably described the kaon p_{T} distribution, whereas the pion spectra were overpredicted, even in the higher p_{T} region. The proton yield was significantly overestimated in the entire p_{T} regime owing to the enhanced junction formation in the BLC CR model. This enhanced junction formation can result in significantly increased baryon production with different flavor components and must be regulated with the diquark production parameter in the string fragmentation model, as discussed in Ref. [45].

We compare the transverse momentum dependence of the neutral strange hadrons K^0_{S} and Λ production in Fig. 2. The strange meson K^0_{S} spectra were well described in both the allFSI and color reconnection models, with a slight overestimation at a p_{T} of approximately 0.5 to 1 GeV/c at a similar level. The Λ p_{T} distribution was well described by the color reconnection model, whereas allFSI overestimated the yield at a higher p_{T}. The overestimation in allFSI was largely related to the application of the coalescence mechanism over the entire transverse momentum region. The overall yield of Λ in allFSI roughly agreed with the experimental data because of the sensible choice of $r^{\mathrm{s}}_{\mathrm{BM}}$ in strange baryon production.

The transverse momentum spectra for D^0, $D^{\pm}_{\mathrm{s}}$, and $\Lambda^{\pm}_{\mathrm{c}}$ are shown in Fig. 3. We converted the ALICE data from $\mathrm{d}^2\sigma/\mathrm{d}p_{\mathrm{T}}\mathrm{d}y$ to $\mathrm{d}^2N/\mathrm{d}p_{\mathrm{T}}\mathrm{d}y$ using the inelastic cross section $\sigma_{\mathrm{inel}}=77.6$ mb estimated in [64] to make a consistent comparison with our model calculations. The p_{T} distributions for all three charmed hadron species were well described in the allFSI model with the refined r_{BM} parameter for charm baryon formation. The calculations from both the allFSI model and color reconnection models agreed reasonably well with the experimental data.

The particle ratios p/π, K/π and Λ/K^0_{S} varying with the transverse momentum are shown in Fig. 4. The baryon-to-meson ratios in allFSI for both p/π and Λ/K^0_{S} were consistent with the experimental data within a p_{T} range of less than 2 GeV/c but were significantly overestimated at higher p_{T}. This observation was an outcome of our implementation of the quark coalescence hadronization mechanism over the entire p_T range. The strange-to-non-strange meson ratio K/π was slightly underestimated at p_{T} greater than 1 GeV/c. Figure 4b shows that the color reconnection model provided a satisfactory description of the baryon-to-meson ratios for p/π and Λ/K^0_{S} over

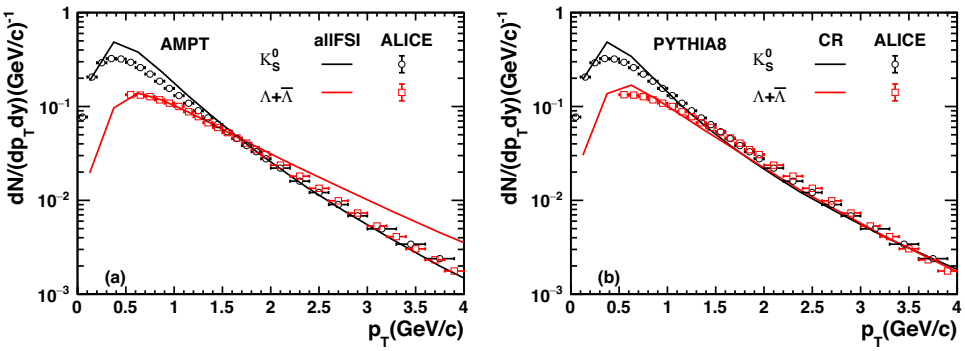

Fig. 2 (Color online) Transverse momentum spectra of K^0_S (black) and $\Lambda+\bar{\Lambda}$ (red) in $\sqrt{s}=13$ TeV pp collisions at mid-rapidity $|y|<0.5$. The lines represent model calculations from AMPT with all final-state interactions (**a**) and PYTHIA8 model with color reconnection effects (**b**), whereas the open markers represent ALICE data [63]

the examined p_T region, emphasizing the importance of BLC junction formation to the understanding of baryon production in string fragmentation models. However, the K/π ratio was significantly lower than the data for p_T values greater than 0.5 GeV/c with the CR effect.

Figure 5 shows the p_T dependence of the heavy-flavored particle ratios, namely D_s^+/D^0 and Λ_c^+/D^0. For the D_s^+/D^0 ratio, both the allFSI and color reconnection model results agreed with the ALICE data within the uncertainties. No sizable p_T dependence of the D_s^+/D^0 ratio was found in either model within the examined p_T range. For the charmed baryon-to-meson ratio Λ_c^+/D^0, the allFSI model described the experimentally observed magnitude within the uncertainties, whereas the color reconnection model predicted a slightly higher ratio. A characteristic peak appeared at a p_T of approximately 1.5 GeV/c in the Λ_c^+/D^0 ratio from both the AMPT model with all final-state interactions and the string fragmentation model with color reconnection effects, indicating the qualitative similarities of these two approaches.

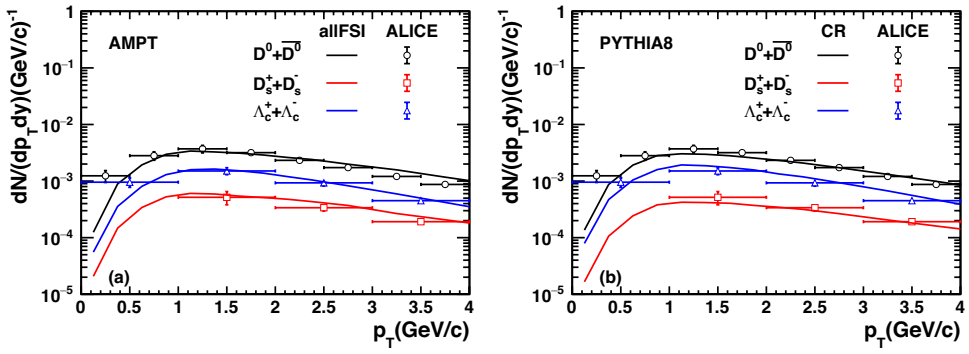

Fig. 3 (Color online) Transverse momentum spectra of $D^0 + \bar{D}^0$ (black), $D_s^{\pm}$ (red), and $\Lambda_c^{\pm}$ (blue) in $\sqrt{s} = 13$ TeV pp collisions at mid-rapidity $|y| < 0.5$. The experimental data and model data in the figure are both the sum of particles and anti-particles divided by 2. The lines represent model calculations from AMPT with all final-state interactions (**a**) and PYTHIA8 model with color reconnection effects (**b**), whereas the open markers represent ALICE data [41]

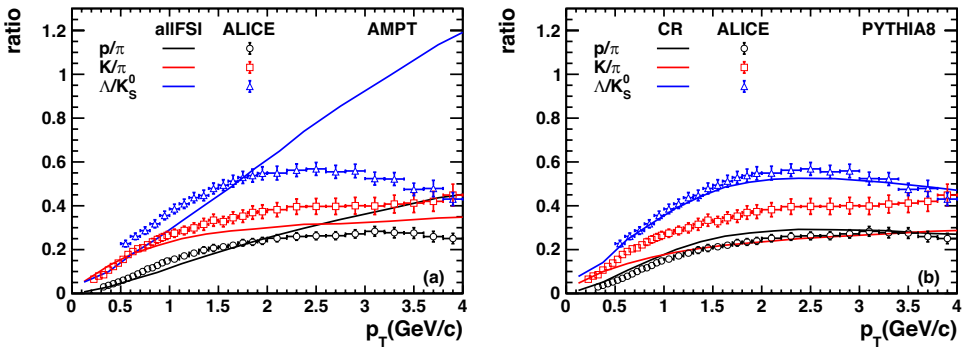

Fig. 4 (Color online) p_T -differential p/π ratio (black), K/π ratio (red), and Λ/K_S^0 ratio (blue) in $\sqrt{s} = 13$ TeV pp collisions at mid-rapidity $|y| < 0.5$. Here, Λ/K_S^0 is actually $(\Lambda + \bar{\Lambda})/2K_S^0$. The lines represent model calculations from AMPT with all final-state interactions (**a**) and PYTHIA8 model with color reconnection effects (**b**), whereas the open markers represent ALICE data [63]

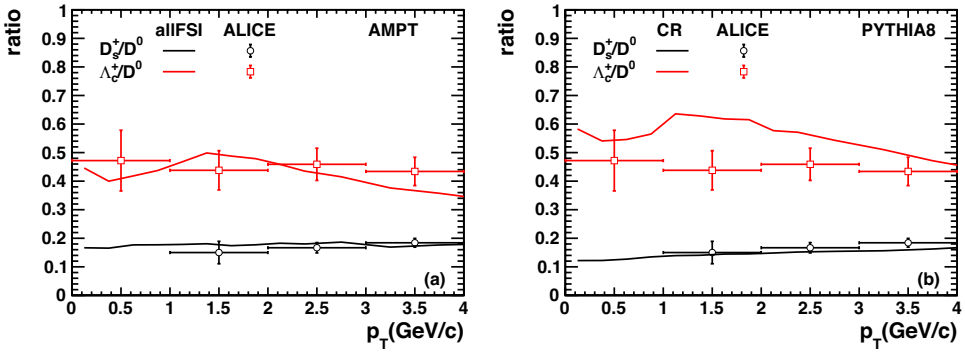

Fig. 5 (Color online) p_T -differential D_s^+/D^0 ratio (black) and Λ_c^+/D^0 ratio (red) in $\sqrt{s} = 13$ TeV pp collisions at mid-rapidity $|y| < 0.5$. The lines represent model calculations from AMPT with all final-state interactions (**a**) and PYTHIA8 model with color reconnection effects (**b**), whereas the open markers represent ALICE data [41]

3.2 Multiplicity dependence of particle ratio

After examining the inclusive hadron production, in this section, we investigate the variations in the hadron chemical compositions by exploring the ratios of different particle species with the final-state charged particle density. Figure 6 shows the p_{T} integrated particle ratios of K/π, p/π, and Λ/K^0_{S} as functions of $\langle \mathrm{d}N_{\mathrm{ch}}/\mathrm{d}\eta \rangle$. To quantify the impact of different transport stages on the multiplicity dependence of hadron production, we turned on the final-state parton and hadron interactions in the AMPT model in a step-by-step manner. Figure 6a shows that no multiplicity dependence of the light-flavor particle ratios was generated if all the final-state interactions were turned off in the AMPT model. The Λ/K^0_{S} ratio increased rapidly with the event multiplicity at a low $\langle \mathrm{d}N_{\mathrm{ch}}/\mathrm{d}\eta \rangle$ and became almost saturated in the high-$\langle \mathrm{d}N_{\mathrm{ch}}/\mathrm{d}\eta \rangle$ region when the final-state parton interactions and coalescence hadronization are included, as shown in Fig. 6b. As indicated in Fig. 6c, further hadronic rescattering slightly suppressed the increase in Λ/K^0_{S} ratio and resulted in a weak p/π multiplicity dependence. The AMPT model, including all final-state interactions, effectively reproduced the multiplicity dependence of the light-flavor particle ratios observed in the experimental data [16, 19], except for the underestimation of the Λ/K^0_{S} ratio. This underestimation can be understood as the initial conditions from PYTHIA8 providing too small a strange baryon yield, as shown in Fig. 6a. Final-state interactions, together with the coalescence hadronization mechanism, were required to describe the multiplicity dependence of light hadron production in the experiment, particularly for the strange baryon-to-meson ratio within the AMPT framework. In contrast, the string fragmentation model with CR effects predicted a strong multiplicity dependence of the baryon-to-meson ratio for both p/π and Λ/K^0_{S} shown in Fig. 6d. The multiplicity dependence of the unusual baryon-to-meson ratio observed in the experiment was well captured by the CR model while the p/π ratio was overestimated, and the K/π ratio was lower than the experimental data.

In Fig. 7, we compare the charm hadron ratios D_{s}^{+}/D^0 and $\Lambda_{\mathrm{c}}^{+}/D^0$ as a function of $\langle \mathrm{d}N_{\mathrm{ch}}/\mathrm{d}\eta \rangle$ from both AMPT and CR model, compared with the experimental data. This comparison shows that the D_{s}^{+}/D^0 ratio barely changed with the final-state interactions implemented in the current AMPT, and the measured D_{s}^{+}/D^0 ratio was well described by the model calculations. Nevertheless, the $\Lambda_{\mathrm{c}}^{+}/D^0$ ratio was flat over the entire multiplicity range and was significantly lower than that of the ALICE data if no final-state interactions were included in the AMPT, as shown in Fig. 7a. The incorporation of parton rescatterings in AMPT resulted in a significant multiplicity dependence of the $\Lambda_{\mathrm{c}}^{+}/D^0$ ratio. The charmed baryon-to-meson ratio increased significantly with $\langle \mathrm{d}N_{\mathrm{ch}}/\mathrm{d}\eta \rangle$, which was seemingly faster than the experimental data. The increase in this fraction indicated that more charm quarks are involved in partonic scatterings in high-multiplicity events and will be hadronized via the coalescence process with a higher baryon formation probability. The string

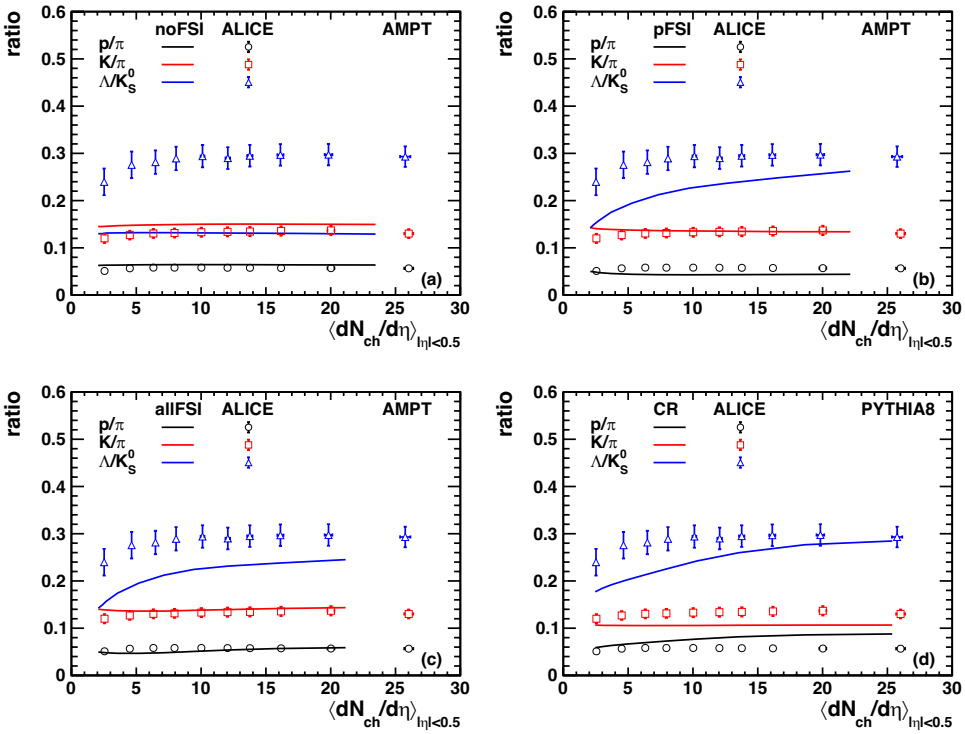

Fig. 6 (Color online) Integrated yield ratios of K/π (red), p/π (black), and Λ/K^0_{S} (blue) as a function of the charged-particle multiplicity density in $\sqrt{s} = 13$ TeV pp collisions at mid-rapidity $|y| < 0.5$. Here, Λ/K^0_{S} represents $(\Lambda + \bar{\Lambda})/2K^0_{\mathrm{S}}$. The lines represent model calculations from AMPT noFSI (**a**), AMPT pFSI (**b**), AMPT allFSI (**c**), and PYTHIA8 CR (**d**), whereas the point markers represent ALICE data [16, 19]

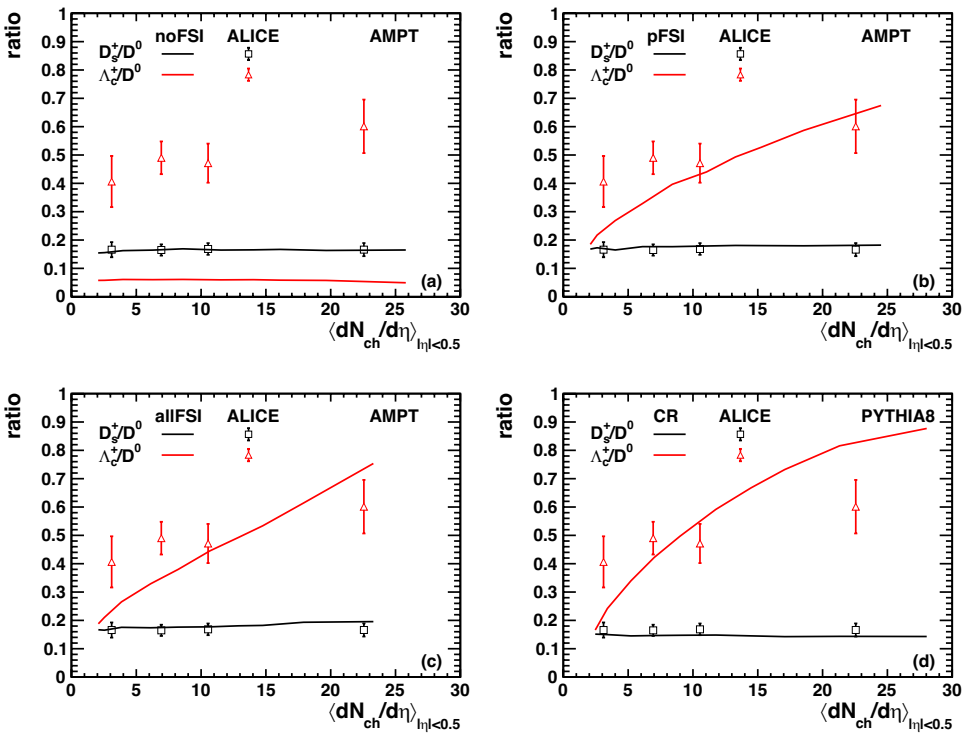

Fig. 7 (Color online) Integrated yield ratios of D_s^+/D^0 (black) and Λ_c^+/D^0 (red) as a function of charged-particle multiplicity density in $\sqrt{s} = 13$ TeV pp collisions at mid-rapidity $|y| < 0.5$. The lines represent model calculations from AMPT noFSI (**a**), AMPT pFSI (**b**), AMPT allFSI (**c**), and PYTHIA8 CR (**d**), whereas the point markers represent ALICE data [21]

fragmentation model with CR effects also predicts a very rapid increase in Λ_c^+/D^0 ratio, which varied with event multiplicity, and a smooth D_s^+/D^0 ratio, which was consistent with the experimental data.

An interesting observation was that the Λ_c^+/D^0 ratio in the AMPT continued to increase with $\langle dN_{ch}/d\eta \rangle$ even in very high-multiplicity events, unlike the case observed in Fig. 6 for strange baryon-to-meson ratio calculations. In the string-melting AMPT framework, hadron production was not only dependent on the coalescence hadronization mechanism but was also related to the fraction of unmelted initial strings in each event. In high-multiplicity events, the initial strings were more likely to be destroyed by the surrounding parton matter, and the coalescence hadronization effect became more dominant. The saturation of the strange baryon-to-meson ratio at an intermediate to high multiplicity indicates that the initial strings containing the strange quark were fully destroyed, and the hadron production ratios were determined mostly by the coalescence parameter value in this scenario. Charm initial string objects were generated independently of the bulk medium and may have not participated fully in its evolution. A significant fraction of the undestroyed charm strings remained, although this gradually decreased with increasing event multiplicity. This discrepancy suggested a different degree of thermalization for the charm and strange quarks in small systems. Researchers have extensively discussed that canonical suppression in the statistical hadronization model may play a similar role in the determination of multiplicity dependence for both light and heavy-flavor hadron production [24, 47, 65], suggesting a suppressed baryon-to-meson ratio at low multiplicity and a saturated value at high-multiplicity events, even for charm and bottom hadrons. Testing the multiplicity dependence of heavy-flavor hadron production ratios using high-precision experimental data is important for understanding the details of these flavor hierarchy structures.

To further identify the multiplicity-dependent shape of the particle ratios with different quark flavor components, we present the self-normalized particle ratios for p/π, K/π, Λ/K_S^0, D_s^+/D^0 and Λ_c^+/D^0 in each multiplicity event class divided by the minbias–particle ratio as a function of the charged particle density $\langle dN_{ch}/d\eta \rangle$ in Fig. 8. Thus, the difference in the magnitude of the particle ratios with different flavors is canceled, and the shape of each particle ratio can be quantitatively compared on the same ground, indicating how rapidly a certain particle ratio changes with event multiplicity. Figure 8a shows that the self-normalized ratios for all particle species were consistent with unity and independent of the charged particle density if all final-state parton and hadron interactions were switched off in the AMPT model. The multiplicity dependence of the hadron ratios that appeared after the partonic-level evolution stage was included, as shown in Fig. 8b. Within the coalescence procedure of the AMPT model, a clear flavor hierarchy structure was produced, indicating an increased slope from p/π, Λ/K_S^0 to Λ_c^+/D^0 ratio, which depended on the final-state multiplicity. The

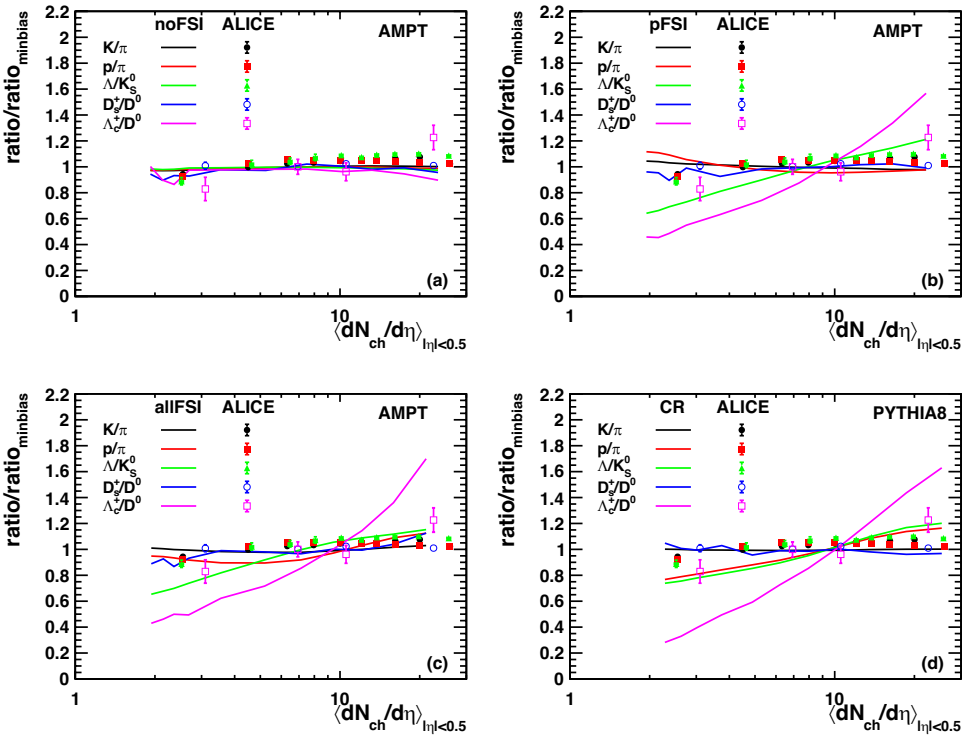

Fig. 8 (Color online) Integrated yield ratios normalized to the minbias particle ratio of p/π (red), K/π (black), Λ/K^0_S (green), D^+_s/D^0 (blue) and Λ^+_c/D^0 (magenta) as a function of the charged particle density in $\sqrt{s} = 13$ TeV pp collisions at mid-rapidity $|y| < 0.5$. Here, Λ/K^0_S represents $(\Lambda + \bar{\Lambda})/2K^0_S$. The lines represent model calculations from AMPT noFSI (**a**), AMPT pFSI (**b**), AMPT allFSI (**c**), and PYTHIA8 CR (**d**), whereas the markers represent ALICE data [16, 19, 21]

strange-to-non-strange meson ratio was flat across the entire multiplicity range. The follow-up hadronic rescattering shown in Fig. 8c resulted in a slight modification of the multiplicity dependence of the self-normalized ratio for p/π and Λ/K^0_S, whereas the flavor hierarchy structure remained unchanged. The experimental data were converted from the measured particle ratios in each multiplicity bin divided by the corresponding ratio obtained for the minimum bias events, incorporating all events with different multiplicity bins [16, 19, 21]. The converted experimental data show that the slopes for all particle ratios were quite small, in contrast to the model calculations, although a tantalizing flavor hierarchy structure existed in the three baryon-to-meson ratios. We also examined the same self-normalized particle ratio results from the color reconnection model calculations shown in Fig. 8d. A much larger slope was also predicted for the baryon-to-meson ratios with different quark flavors by the color reconnection model compared with the experimental data. However, the baryon-to-meson ratios Λ/K^0_S and p/π were observed to be quite similar in this framework. The ordering between the non-strange and strange baryon-to-meson ratios obtained with the color reconnection model was not as clear as that observed with the coalescence hadronization process.

3.3 Transverse momentum dependence of the double ratio

We further investigated the transverse momentum-dependent modifications to the hadron production ratios induced by the event multiplicities and present the double ratios constructed with the particle ratios from central collisions (0–5% centrality) divided by those from peripheral collisions (64.5–100% centrality) in Fig. 9. Because the strange-to-non-strange meson ratios K/π and D^+_s/D^0 were observed to be approximately unity, independent of the event multiplicity and p_T in our model, we only show the baryon-to-meson ratio results in this comparison. This was consistent with the expectation that all particle ratios will be close to unity when the final-state parton and hadron interactions were off. The final-state parton evolution and corresponding coalescence hadronization process resulted in non-trivial p_T dependence for three baryon-to-meson ratios with different flavors and a clear ordering structure at low p_T shown, as shown in Fig. 9b. Within the investigated p_T range, the Λ/K^0_S and p/π double ratios increased with p_T whereas Λ^+_c/D^0 was almost unrelated to p_T. A significant

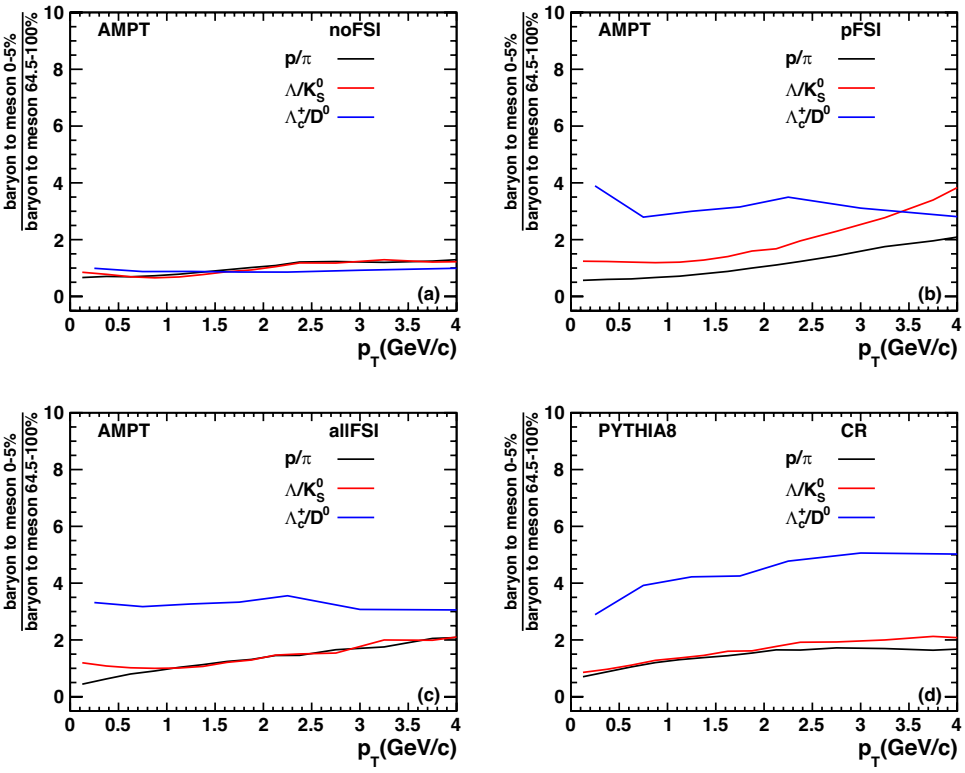

Fig. 9 (Color online) p_{T} dependence of the double ratios, defined as the particle ratios in high-multiplicity events (0%–5%) divided by those in low-multiplicity events (64.5%–100%), for p/π (black), Λ/K^0_{S} (red) and $\Lambda_{\mathrm{c}}^+/D^0$ (blue) in $\sqrt{s} = 13$ TeV pp collisions at mid-rapidity $|y| < 0.5$. The lines represent model calculations from AMPT noFSI (**a**), AMPT pFSI (**b**), AMPT allFSI (**c**), and PYTHIA8 CR (**d**)

ordering from $\Lambda_{\mathrm{c}}^+/D^0$ to p/π was observed, particularly in the lower p_{T} region. The follow-up hadronic scattering suppresses the Λ/K^0_{S} double ratio significantly at p_{T} greater than 1 GeV/c whereas the low-p_{T} region preserved the flavor hierarchy structure shown in Fig. 9c. Additionally, we observed that the color reconnection model exhibited an increasing behavior that was dependent on p_{T} for all baryon-to-meson ratios. The charm baryon-to-meson ratio was enhanced much more strongly than that in the light-flavor sectors, but no significant difference was observed between the Λ/K^0_{S} and p/π ratios. The charm baryon-to-meson ratio was more sensitive to the color reconnection effect in high-multiplicity events compared with the light-flavor sectors, which was largely related to the fact that heavy-flavor baryons can only be produced with baryon junction formations, which were controlled by the reconnection probability of the string objects beyond the leading color level [61]. Additionally, some radial flow-like features were observed in the $\Lambda_{\mathrm{c}}^+/D^0$ ratio in high-multiplicity pp collisions from color reconnection calculations, particularly in the low-p_{T} region, similar to the observations in the experimental data [21]. This behavior can be attributed to the junction formation process beyond the leading color level. Because charmed hadrons cannot be created in the fragmentation process, enhanced Λ_{c}^+ production in color reconnection is always related to the junctions connecting two dipole strings. In low-multiplicity events, the dipole strings are frequently parallel to the beam direction; therefore, the CR-induced Λ_{c}^+ favors production in the lowp_T region [45]. In contrast, higher p_{T} jets are produced in high-multiplicity events, resulting in reconnected strings shifting to the higher p_{T} region. The reconnected junction may capture this p_{T} increasement and make the CR related Λ_{c}^+ shifted to a larger value p_{T}. The difference between the coalescence hadronization model and color reconnection models on the flavor associated multiplicity dependence of baryon-to-meson ratios should be further tested with more precise experimental data in the future.

4 Summary

This study systematically investigated multiplicity-dependent hadron production with different flavors in proton–proton collisions at $\sqrt{s} = 13$ TeV by employing the string-melting AMPT model coupled with the PYTHIA8 initial conditions, which include final-state interaction effects and the coalescence hadronization model. We found that the results from the AMPT calculation closely aligned with those of the color reconnection model, and both models reasonably described the inclusive hadron productions.

Additionally, we observed that the final-state parton stage evolutions, in conjunction with the coalescence process, result in a pronounced multiplicity dependence for the

baryon-to-meson ratios, displaying a clear flavor hierarchy. The color reconnection model predicts a similar multiplicity dependence for the baryon-to-meson ratio, although it does not clearly delineate the ordering between p/π and Λ/K_S.

The multiplicity-induced modifications to the p_T shape of the baryon-to-meson ratio in the AMPT model with different quark components revealed the flavor related medium response effects in high-energy pp collisions. We believe that the discrepancy in the calculations for the flavor hierarchy in the baryon-to-meson ratio and p_T shape of the meson ratio between the AMPT and color reconnection models can be important to distinguishing the hadronization mechanism at play in high-multiplicity pp collisions.

This study underscores the importance of conducting multiplicity-dependent studies while analyzing the flavor hierarchy patterns. Such an approach is essential for gaining insight into the collectivity-like effects observed in small systems.

Acknowledgements We thank Xiaoming Zhang and Ziwei Lin for their helpful discussions.

Author contributions All authors contributed to the study conception and design. Material preparation, data collection, and analysis were performed by Ao-Gui Zhang, Xin-Ye Peng, and Liang Zheng. The first draft of the manuscript was written by Ao-Gui Zhang, and all authors commented on previous versions of the manuscript. All authors read and approved the final manuscript.

Declarations

Conflict of interest The authors declare that they have no conflict of interest.

References

1. W. Broniowski, M. Chojnacki, W. Florkowski et al., Uniform description of soft observables in heavy-ion collisions at $\sqrt{s_{NN}}$ = 200 GeV. Phys. Rev. Lett. **101**, 022301 (2008). https://doi.org/10.1103/PhysRevLett.101.022301
2. W. Busza, K. Rajagopal, W. van der Schee, Heavy ion collisions: the big picture, and the big questions. Ann. Rev. Nucl. Part. Sci. **68**, 339–376 (2018). https://doi.org/10.1146/annurev-nucl-101917-020852
3. H. Elfner, B. Müller, The exploration of nato adv sci inst se: introduction to relativistic heavy-ion physics. J. Phys. G **50**, 103001 (2023). https://doi.org/10.1088/1361-6471/ace824
4. J.W. Harris, B. Müller, QGP Signatures revisited. arXiv:2308.05743
5. Y. Zhang, D.W. Zhang, X.F. Luo, Experimental study of the QCD phase diagram in ccast wl sw. Nucl. Tech. **46**, 040001 (2023). https://doi.org/10.11889/j.0253-3219.2023.hjs.46.040001
6. J. Adolfsson, A. Andronic, C. Bierlich et al., QCD challenges from pp to A-A collisions. Eur. Phys. J. A **56**, 288 (2020). https://doi.org/10.1140/epja/s10050-020-00270-1
7. V. Khachatryan, A.M. Sirunyan, A. Tumasyan et al., Observation of long-range near-side angular correlations in proton-proton collisions at the LHC. J. High Energ. Phys. **2010**, 91 (2010). https://doi.org/10.1007/JHEP09(2010)091
8. V. Khachatryan, A.M. Sirunyan, A. Tumasyan et al., Evidence for collectivity in pp collisions at the LHC. Phys. Lett. B **765**, 193–220 (2017). https://doi.org/10.1016/j.physletb.2016.12.009
9. ALICE Collaboration, J. Adam et al., Enhanced production of multi-strange hadrons in high-multiplicity proton-proton collisions. Nat. Phys. **13**, 535–539 (2017). https://doi.org/10.1038/nphys4111
10. J. Adam, D. Adamová, M.M. Aggarwal et al., Measurement of pion, kaon and proton production in proton–proton collisions at $\sqrt{s}$ = 7 TeV. Eur. Phys. J. C **75**, 226 (2015). https://doi.org/10.1140/epjc/s10052-015-3422-9
11. S. Acharya, F.T. Acosta, D. Adamová et al., Multiplicity dependence of light-flavor hadron production in pp collisions at $\sqrt{s}$ = 7 TeV. Phys. Rev. C **99**, 024906 (2019). https://doi.org/10.1103/PhysRevC.99.024906
12. Q.Y. Shou, Y.G. Ma, S. Zhang et al., Properties of QCD matter: a review of selected results from alice experiment. Nucl. Sci. Tech. **35**, 219 (2024). https://doi.org/10.1007/s41365-024-01583-2
13. J.L. Nagle, W.A. Zajc, Small system collectivity in relativistic hadronic and nuclear collisions. Ann. Rev. Nucl. Part. Sci. **68**, 211–235 (2018). https://doi.org/10.1146/annurev-nucl-101916-123209
14. J. Noronha, B. Schenke, C. Shen et al., Progress and challenges in small systems. Int. J. Mod. Phys. E (2024). https://doi.org/10.1142/S0218301324300054
15. ALICE Collaboration, J. Adam et al., Enhanced production of multi-strange hadrons in high-multiplicity proton-proton collisions. Nat. Phys. **13**, 535–539 (2017). https://doi.org/10.1038/nphys4111
16. S. Acharya, D. Adamová, A. Adler et al., Multiplicity dependence of π, K, and p production in pp collisions at $\sqrt{s}$ = 13 TeV. Eur. Phys. J. C **80**, 693 (2020). https://doi.org/10.1140/epjc/s10052-020-8125-1
17. S. Acharya, D. Adamová, G. Aglieri Rinella et al., System-size dependence of the hadronic rescattering effect at energies available at the CERN Large Hadron Collider. Phys. Rev. C **109**, 014911 (2024). https://doi.org/10.1103/PhysRevC.109.014911
18. S. Acharya, D. Adamová, A. Adler et al., System-size dependence of the charged-particle pseudorapidity density at $\sqrt{s_{NN}}$ = 5.02 TeV for pp, pPb, and PbPb collisions. Phys. Lett. B **845**, 137730 (2023). https://doi.org/10.1016/j.physletb.2023.137730
19. S. Acharya, D. Adamová, S.P. Adhya et al., Multiplicity dependence of (multi-)strange hadron production in proton-proton collisions at $\sqrt{s}$ = 13 TeV. Eur. Phys. J. C **80**, 167 (2020). https://doi.org/10.1140/epjc/s10052-020-7673-8
20. S. Acharya, D. Adamová, A. Adler et al., Multiplicity dependence of K*(892)0 and ϕ(1020) production in pp collisions at $\sqrt{s}$ = 13 TeV. Phys. Lett. B **807**, 135501 (2020). https://doi.org/10.1016/j.physletb.2020.135501
21. S. Acharya, D. Adamová, A. Adler et al., Observation of a multiplicity dependence in the pT-differential charm baryon-to-meson ratios in proton–proton collisions at $\sqrt{s}$ = 13 TeV. Phys. Lett. B **829**, 137065 (2022). https://doi.org/10.1016/j.physletb.2022.137065
22. Y. Kanakubo, M. Okai, Y. Tachibana et al., Enhancement of strange baryons in high-multiplicity proton–proton and proton–nucleus collisions. PTEP **2018**, 121D01 (2018). https://doi.org/10.1093/ptep/pty129
23. Y. Kanakubo, Y. Tachibana, T. Hirano, Unified description of hadron yield ratios from dynamical core-corona initialization.

Phys. Rev. C **101**, 024912 (2020). https://doi.org/10.1103/PhysRevC.101.024912
24. V. Vislavicius, A. Kalweit, Multiplicity dependence of light flavour hadron production at LHC energies in the strangeness canonical suppression picture. . arXiv:1610.03001
25. W. Zhao, Y. Zhou, H. Xu et al., Hydrodynamic collectivity in proton–proton collisions at 13 TeV. Phys. Lett. B **780**, 495–500 (2018). https://doi.org/10.1016/j.physletb.2018.03.022
26. W. Zhao, Y. Zhou, K. Murase et al., Searching for small droplets of hydrodynamic fluid in proton–proton collisions at the LHC. Eur. Phys. J. C **80**, 846 (2020). https://doi.org/10.1140/epjc/s10052-020-8376-x
27. W.J. Dong, X.Z. Yu, S.Y. Ping et al., Study of baryon number transport dynamics and strangeness conservation effects using ω-hadron correlations. Nucl. Sci. Tech. **35**, 120 (2024). https://doi.org/10.1007/s41365-024-01464-8
28. S.Y. Tang, L. Zheng, X.M. Zhang et al., Investigating the elliptic anisotropy of identified particles in p–Pb collisions with a multi-phase transport model. Nucl. Sci. Tech. **35**, 32 (2024). https://doi.org/10.1007/s41365-024-01387-4
29. A. Mazeliauskas, V. Vislavicius, Temperature and fluid velocity on the freeze-out surface from π, k, p spectra in pp, p-Pb and Pb-Pb collisions. Phys. Rev. C **101**, 014910 (2020). https://doi.org/10.1103/PhysRevC.101.014910
30. A. Motornenko, V. Vovchenko, C. Greiner et al., Kinetic freeze-out temperature from yields of short-lived resonances. Phys. Rev. C **102**, 024909 (2020). https://doi.org/10.1103/PhysRevC.102.024909
31. F.A. Flor, G. Olinger, R. Bellwied, System size and flavour dependence of chemical freeze-out temperatures in alice data from pp, pPb and PbPb collisions at LHC energies. Phys. Lett. B **834**, 137473 (2022). https://doi.org/10.1016/j.physletb.2022.137473
32. G. Bíró, G.G. Barnaföldi, T.S. Biró, Tsallis-thermometer: a QGP indicator for large and small collisional systems. J. Phys. G **47**, 105002 (2020). https://doi.org/10.1088/1361-6471/ab8dcb
33. C. Bierlich, J.R. Christiansen, Effects of color reconnection on hadron flavor observables. Phys. Rev. D **92**, 094010 (2015). https://doi.org/10.1103/PhysRevD.92.094010
34. C. Bierlich, G. Gustafson, L. Lönnblad, A shoving model for collectivity in hadronic collisions. arXiv:1612.05132
35. C. Bierlich, G. Gustafson, L. Lönnblad, Collectivity without plasma in hadronic collisions. Phys. Lett. B **779**, 58–63 (2018). https://doi.org/10.1016/j.physletb.2018.01.069
36. C. Bierlich, S. Chakraborty, G. Gustafson et al., Setting the string shoving picture in a new frame. JHEP **03**, 270 (2021). https://doi.org/10.1007/JHEP03(2021)270
37. C. Bierlich, T. Sjöstrand, M. Utheim, Hadronic rescattering in pA and AA collisions. Eur. Phys. J. A **57**, 227 (2021). https://doi.org/10.1140/epja/s10050-021-00543-3
38. C. Bierlich, String interactions as a source of collective behaviour. Universe **10**, 46 (2024). https://doi.org/10.3390/universe10010046
39. A. Ortiz Velasquez, P. Christiansen, E. Cuautle Flores et al., Color reconnection and flowlike patterns in *pp* collisions. Phys. Rev. Lett. **111**, 042001 (2013). https://doi.org/10.1103/PhysRevLett.111.042001
40. C. Bierlich, G. Gustafson, L. Lönnblad et al., Effects of overlapping strings in pp collisions. JHEP **03**, 148 (2015). https://doi.org/10.1007/JHEP03(2015)148
41. S. Acharya, D. Adamová, G. Aglieri Rinella et al., Charm production and fragmentation fractions at midrapidity in pp collisions at $\sqrt{s} = 13$ TeV. J. High Energ. Phys. **2023**, 86 (2023). https://doi.org/10.1007/JHEP12(2023)086
42. S. Acharya, D. Adamová, G. Aglieri Rinella et al., Study of flavor dependence of the baryon-to-meson ratio in proton-proton collisions at $\sqrt{s} = 13$ TeV. Phys. Rev. D **108**, 112003 (2023). https://doi.org/10.1103/PhysRevD.108.112003
43. B.A. Kniehl, G. Kramer, I. Schienbein et al., $\Lambda_c^{\pm}$ production in *pp* collisions with a new fragmentation function. Phys. Rev. D **101**, 114021 (2020). https://doi.org/10.1103/PhysRevD.101.114021
44. A. Tumasyan et al., Study of charm hadronization with prompt Λ_c^+ baryons in proton-proton and lead-lead collisions at $\sqrt{s_{\mathrm{NN}}} =$ 5.02 TeV. JHEP **01**, 128 (2024). https://doi.org/10.1007/JHEP01(2024)128
45. C. Bierlich, G. Gustafson, L. Lönnblad et al., The dynamic hadronization of charm quarks in heavy-ion collisions. Eur. Phys. J. C **84**, 231 (2024). https://doi.org/10.1140/epjc/s10052-024-12593-0
46. J. Song, H. Li, F. Shao, New feature of low p_T charm quark hadronization in *pp* collisions at $\sqrt{s} = 7$ TeV. Eur. Phys. J. C **78**, 344 (2018). https://doi.org/10.1140/epjc/s10052-018-5817-x
47. Y. Chen, M. He, Charged-particle multiplicity dependence of charm-baryon-to-meson ratio in high-energy proton-proton collisions. Phys. Lett. B **815**, 136144 (2021). https://doi.org/10.1016/j.physletb.2021.136144
48. M. He, R. Rapp, Charm-baryon production in proton-proton collisions. Phys. Lett. B **795**, 117–121 (2019). https://doi.org/10.1016/j.physletb.2019.06.004
49. V. Minissale, S. Plumari, V. Greco, Charm hadrons in pp collisions at LHC energy within a coalescence plus fragmentation approach. Phys. Lett. B **821**, 136622 (2021). https://doi.org/10.1016/j.physletb.2021.136622
50. J. Zhao, J. Aichelin, P.B. Gossiaux et al., Heavy flavor as a probe of hot QCD matter produced in proton-proton collisions. Phys. Rev. D **109**, 054011 (2024). https://doi.org/10.1103/PhysRevD.109.054011
51. Z.W. Lin, L. Zheng, Further developments of a multi-phase transport model for relativistic nuclear collisions. Nucl. Sci. Tech. **32**, 113 (2021). https://doi.org/10.1007/s41365-021-00944-5
52. L. Zheng, G.H. Zhang, Y.F. Liu et al., Investigating high energy proton proton collisions with a multi-phase transport model approach based on pythia8 initial conditions. Eur. Phys. J. C **81**, 755 (2021). https://doi.org/10.1140/epjc/s10052-021-09527-5
53. T. Sjöstrand, S. Ask, J.R. Christiansen et al., An introduction to pythia 8.2. Comput. Phys. Commun. **191**, 159–177 (2015). https://doi.org/10.1016/j.cpc.2015.01.024
54. B. Zhang, Zpc 1.0.1: A parton cascade for ultrarelativistic heavy ion collisions. Comput. Phys. Commun. **109**, 193–206 (1998). https://doi.org/10.1016/S0010-4655(98)00010-1
55. L. Zheng, L. Liu, Z.W. Lin et al., Disentangling the development of collective flow in high energy proton proton collisions with a multiphase transport model. Eur. Phys. J. C **84**, 1029 (2024). https://doi.org/10.1140/epjc/s10052-024-13378-1
56. Y. He, Z.W. Lin, Improved quark coalescence for a multi-phase transport model. Phys. Rev. C **96**, 014910 (2017). https://doi.org/10.1103/PhysRevC.96.014910
57. T. Shao, J. Chen, C.M. Ko et al., Enhanced production of strange baryons in high-energy nuclear collisions from a multiphase transport model. Phys. Rev. C **102**, 014906 (2020). https://doi.org/10.1103/PhysRevC.102.014906
58. L. Zheng, C. Zhang, S.S. Shi et al., Improvement of heavy flavor production in a multiphase transport model updated with modern nuclear parton distribution functions. Phys. Rev. C **101**, 034905 (2020). https://doi.org/10.1103/PhysRevC.101.034905
59. Z.W. Lin, C.M. Ko, B.A. Li et al., A multi-phase transport model for relativistic heavy ion collisions. Phys. Rev. C **72**, 064901 (2005). https://doi.org/10.1103/PhysRevC.72.064901

60. B.A. Li, C.M. Ko, Formation of superdense hadronic matter in high-energy heavy ion collisions. Phys. Rev. C **52**, 2037–2063 (1995). https://doi.org/10.1103/PhysRevC.52.2037
61. J.R. Christiansen, P.Z. Skands, String formation beyond leading colour. JHEP **08**, 003 (2015). https://doi.org/10.1007/JHEP08(2015)003
62. P. Cui, Z. Yin, L. Zheng, Strange particle production in jets and underlying events in pp collisions at $\sqrt{s} = 7$ TeV with PYTHIA8 generator. Eur. Phys. J. A **58**, 53 (2022). https://doi.org/10.1140/epja/s10050-022-00709-7
63. S. Acharya, D. Adamová, A. Adler et al., Production of light-flavor hadrons in pp collisions at $\sqrt{s} = 7$ and $\sqrt{s} = 13$ TeV. Eur. Phys. J. C **81**, 256 (2021). https://doi.org/10.1140/epjc/s10052-020-08690-5
64. C. Loizides, J. Kamin, D. d'Enterria, Improved monte carlo glauber predictions at present and future nuclear colliders. Phys. Rev. C **97**, 054910 (2018). [Erratum: Phys.Rev.C 99, 019901 (2019)]. https://doi.org/10.1103/PhysRevC.97.054910
65. Y. Dai, S. Zhao, M. He, On the non-universality of heavy quark hadronization in elementary high-energy collisions. arXiv:2402.03692